Improved hemostatic effects by Fe^{3+} modified biomimetic PLLA cotton-like mat via sodium alginate grafted with dopamine

Caili Lv [a,b], Linlong Li [a,c], Zixue Jiao [a], Huanhuan Yan [a,b], Zongliang Wang [a], Zhenxu Wu [a], Min Guo [a], Yu Wang [a,**], Peibiao Zhang [a,b,*]

[a] *Key Laboratory of Polymer Ecomaterials, Changchun Institute of Applied Chemistry, Chinese Academy of Sciences, 5625 Renmin Street, Changchun, 130022, PR China*
[b] *School of Applied Chemistry and Engineering, University of Science and Technology of China, 96 Jinzhai Road, Hefei, Anhui, 230026, PR China*
[c] *University of Chinese Academy of Sciences, 19 Yuquan Road, Beijing, 100049, PR China*

ARTICLE INFO

ABSTRACT

The development of an excellent, bioabsorbable hemostatic material for deep wound remains a challenge. In this work, a biodegradable cotton-like biomimetic fibrous mat of poly (L-lactic acid) (PLLA) was made by melt spinning. Subsequently, SD composite was prepared by cross-linking sodium alginate (SA) with dopamine (DA). It was immobilized on the fibre surface, which inspired by mussel byssus. Finally, Fe^{3+} was loaded onto the 0.5SD/PLLA composite by chelation with the carboxyl of alginate and phenolic hydroxy of dopamine. The haemostasis experiment found that the hemostatic time 47 s in vitro. However, the bleeding volume was 0.097 g and hemostatic time was 23 s when $20Fe^{3+}$-0.5SD/PLLA was applied in the haemostasis of the rat liver. As a result of its robust hydrophilicity and bouffant cotton-like structure, it could absorb a large water from blood, which could concentrate the component of blood and reduce the clotting time. Furthermore, the addition of Fe^{3+} in the 0.5SD/PLLA had a significant effect on improve hemostatic property. It also displayed excellent antibacterial property for *Escherichia coli* and *Staphylococcus aureus*. Notably, it possesses superior hemocompatibility, cytocompatibility and histocompatibility. Hence, $20Fe^{3+}$-0.5SD/PLLA has high potential application in haemostasis for clinical settings due to its outstanding properties.

1. Introduction

Excessive haemorrhage is a matter of concern for military traumas, surgical operations and other civilian accidents [1,2], and uncontrolled haemorrhage is the main reason of pre-hospital death [3]. Reducing suffering and mortality of patients is an urgent need that needs to be addressed immediately [4]. In addition, an ideal clinical hemostatic agent should have effective antibacterial property to resist infection. Currently, various hemostatic materials, including hemostatic microparticles [5], cellulose−halloysite nanocomposite fibers [6], gauze [7] and hemostatic hydrogel [8], have been studied for rapid and effective haemostasis. For example, hemostatic microparticles are commonly used in the treatment of venous, capillary and arteriolar bleeding by pressure [5,9]. Thus, many traditional hemostatic agents fail to meet the design requirements for deep wounds, abdominal surgery and punctured

wound haemorrhage. It is difficult to achieve haemostasis because plenty of microparticles are needed to fill the wound, which obviously wastes treatment time. Though silica foams decorated with silver ions achieved significant result of haemostasis for deep wound haemorrhage and antibacterial properties, which causes severe rejection reactions due to its poor biocompatibility and degradability if any residues remain in the body [10]. On the other hand, collagen sponge has been reported to possess excellent hemostatic effect [11–13]. However, it is costly, and patients cannot easily afford high medical costs. Therefore, the preparation of biocompatible, antibacterial and economical hemostatic materials for deep wounds is a major challenge.

Bioresorbable and non-toxic synthetic biopolymers are often used as hemostatic scaffolds [14–16]. For example, Hu et al. reported that poly (L-lactic acid) (PLLA) braided wires coated with chitosan have super pro-hemostatic activity [17]. While, the mini-type braiding method is

complicated and the production process is slow, making it difficult to meet high demand. In addition, PLLA nano-fabric membrane containing fibringen is prepared by electrospinning, which detects excellent hemostatic effects [18]. However, residual organic solvents in fibres by electrospinning are toxic to cellular activity, which restricts the application of electrosping fibrous scaffolds in clinical [19,20]. Melt spinning of polymers is the most popular used method for manufacturing fibres [21–23]. This melt spinning has several important advantages compared with electrospinning. The fiber made by melt spinning overcome the residual organic solvent in fibres of traditional electrospinning. Electrospinning technology can only produce fibre membrane. Whereas, melt spinning technology can produce fibre mat with similar three-dimensional structure of cotton, which can be used to fill deep wounds. The melt spinning technology is simple and can avoid the pollution caused by volatilization of organic solvents compared with electrospinning technology. The fibre mat with similar three-dimensional structure of cotton is a good choice for the hemostasis of deep wounds, but it has not been applied to the study of hemostatic properties.

Hemostatic materials require excellent hydrophilicity, water absorption property and the ability to quickly absorb blood exudate so that clotting factor, platelet and red blood cells can gather quickly to promote thrombus formation [24]. Alginate (Alg) is an excellent hemostatic material because of its excellent biocompatibility, hydrophilicity and relatively low cost; Furthermore, the active group of carboxyl can be grafted with other materials [25,26]. when Alg microspheres are introduced into the chitosan (CS) sponge, blood coagulation can be significantly improved, and the bleeding time of CS/Alg 10 was obviously reduced compared with CS sponge [27]. A sodium alginate (SA) coated three-dimensional silica hemostatic sponge shows that hemostasis is achieved and the amount of bleeding is significantly reduced compared with silica nanofibers [28]. Moreover, to further improve the hemostatic effect, some inorganic ions with hemostatic property are usually added to hemostatic materials for synergistic effects. In 1943, the hemostatic effectiveness of $FeCl_3$ in the brain, viscera and superior sagittal sinus was studied and good hemostatic effect was obtained [29, 30]. Nechipurenko et al. reported that the translocation of procoagulant platelet by using $FeCl_3$ to promote thrombosis [31]. Furthermore, the quinone groups formed by Fe^{3+} oxidation with the catechol group have superior antibacterial property [32]. Hence, how to modify sodium alginate and Fe^{3+} on the surface of fibrous of PLLA cotton mat with synergistically hemostatic and antibacterial property is a challenge.

Inspired by mussel-adhesion phenomena in nature [33]. Dopamine (DA) can form a polydopamine (PDA)-coating on the surface of polymers, metals and metal oxides [34] when the materials are simply immersed in alkaline solution of DA. In this work, the amino group of DA is chemically cross-linked with the carboxyl group of sodium alginate (SA), then form a sodium alginate/dopamine composite (SD), which provides a method to bind SA to the surface of the PLLA fibre mat. Finally, Fe^{3+} was cross-linked with SA and PDA. Moreover, the catechol-Fe^{3+}-catechol key is stable under acid, alkali and neutral environments [35], thus it can form a stable coating on the surface of PLLA fibre. Its physical/chemical structure, hydrophilicity, water absorption ability, in vitro and vivo hemostatic property, cytocompatibility, hemocompatibility and antibacterial activity were systematically characterised.

2. Experimental section

2.1. Materials

Iron chloride hexahydrate (98%; $FeCl_3 \cdot 6H_2O$) was purchased from Beijing Chemical Works (Beijing, China). DA was bought from Adamas Reagent Co, Ltd. L-lactic (LA) was procured from Purac (Netherlands). SA was obtained from Sinopharm Chemical Reagent Co (Shanghai, China). 4-Morpholineethanesulfonic acid (MES), *N*-hydroxysuccinimide

(NHS) and carbodiimide hydrochloride (EDC·HCl) were purchased from Energy Chemical. Triton X-100 was bought from Aladdin Industrial Corporation. Details of other materials used are available in Materials and Methods, Supporting Information (SI).

2.2. Synthesis of polymer

PLLA polymer was synthesised in our laboratory according to a previous method (see the SI). The average molecular weight of PLLA was 43,000, and DSC revealed that the melting temperature of the PLLA polymer was 174 °C.

2.3. Preparation of PLLA melt spinning mat

The dried PLLA powder was added into the preheated heating tube with the temperature 10 °C higher than the melting temperature of PLLA polymer and heated for 5–8 min. Subsequently, nitrogen was injected via the top of heating tube charged at a high voltage. When the melt flowed out uniformly, hot air (450 °C, which was higher than the melting temperature of polymer) was added on the lower end of the spinning nozzle. The melt of PLLA was elongated by high-speed hot air, and the melt travelled to the collector that was wire mesh (Fig. 1(1)).

2.4. Preparation of polydopamine-alginate composite (SD)

The SD composite was prepared based on published methods [36]. In brief, the solution with different concentrations of SA (0.1%, 0.3% and 0.5%; w/V%) was obtained by dissolving SA in deionised water at room temperature. When the SA powders were completely dissolved, the EDC/NHS (the ratio of EDC to NHS monomer was 1:1) was added to SA solution with the molar ratio of EDC to SA repeating unit of 1:2.5 to activate the carboxyl groups of SA. MES (a buffer agent, 29 mM) was added, and the blending solution above was stirred for about 10 min to form a uniform solution. Finally, the pH of the uniform blending solution was adjusted to 5.5. After 2 h, DA was added to activate the SA solution with the mass ratio of DA to SA of 1:10, and the resulting solution was stirred at room temperature for 12 h. To remove the unreacted coupling reagents and micro-molecule, the obtained solution was dialysed with a dialysis bag (molecular weight cut off = 3500 Da) for 72 h, and deionised water was replaced every 3 h (see Scheme 1(2) and Scheme 2(1)).

2.5. Preparation of SD/PLLA and Fe^{3+}-SD/PLLA composite

The SD composite was coated on the PLLA melt spinning mat according to our previous study [37]. As shown in Scheme 2 (2), the PLLA melt spinning mat was soaked in SD solution (2 mg/mL in 50 mM, Tris·HCl, pH 8.0) for 2 h under ambient temperature (SD/PLLA). Subsequently, the SD/PLLA composite was placed on the barbed wire to leach the excess SD solution and rinsed three times with deionised water to remove free SD. Finally, the SD/PLLA composites were stored in the refrigerator (−80 °C) for 10 min and freeze dried for 2 days.

$FeCl_3 \cdot 6H2O$ was dissolved in deionised water with different concentrations (5, 10 and 20 mM) at room temperature. The 0.5SD/PLLA composites were immersed in $FeCl_3 \cdot 6H2O$ solution for 18 h (Fe^{3+}-0.5SD/PLLA) and then rinsed three times with deionised water (Scheme 2 (3)). Subsequently, the composite materials were placed in the refrigerator (−80 °C) for 10 min and then dried for 2 days by using a freezer dryer.

2.6. Characterization

The chemical structure was measured by Fourier transform infrared spectroscopy (FT-IR; PerkinElmer, FTIR-2000). X-ray photoelectron spectroscopy (XPS; Thermo ESCALAB 250) was utilised to detect the SD/PLLA composites. The morphology of all the composites was observed by scanning electron microscopy (SEM; Philips XL30 ESEM FEG, Japan),
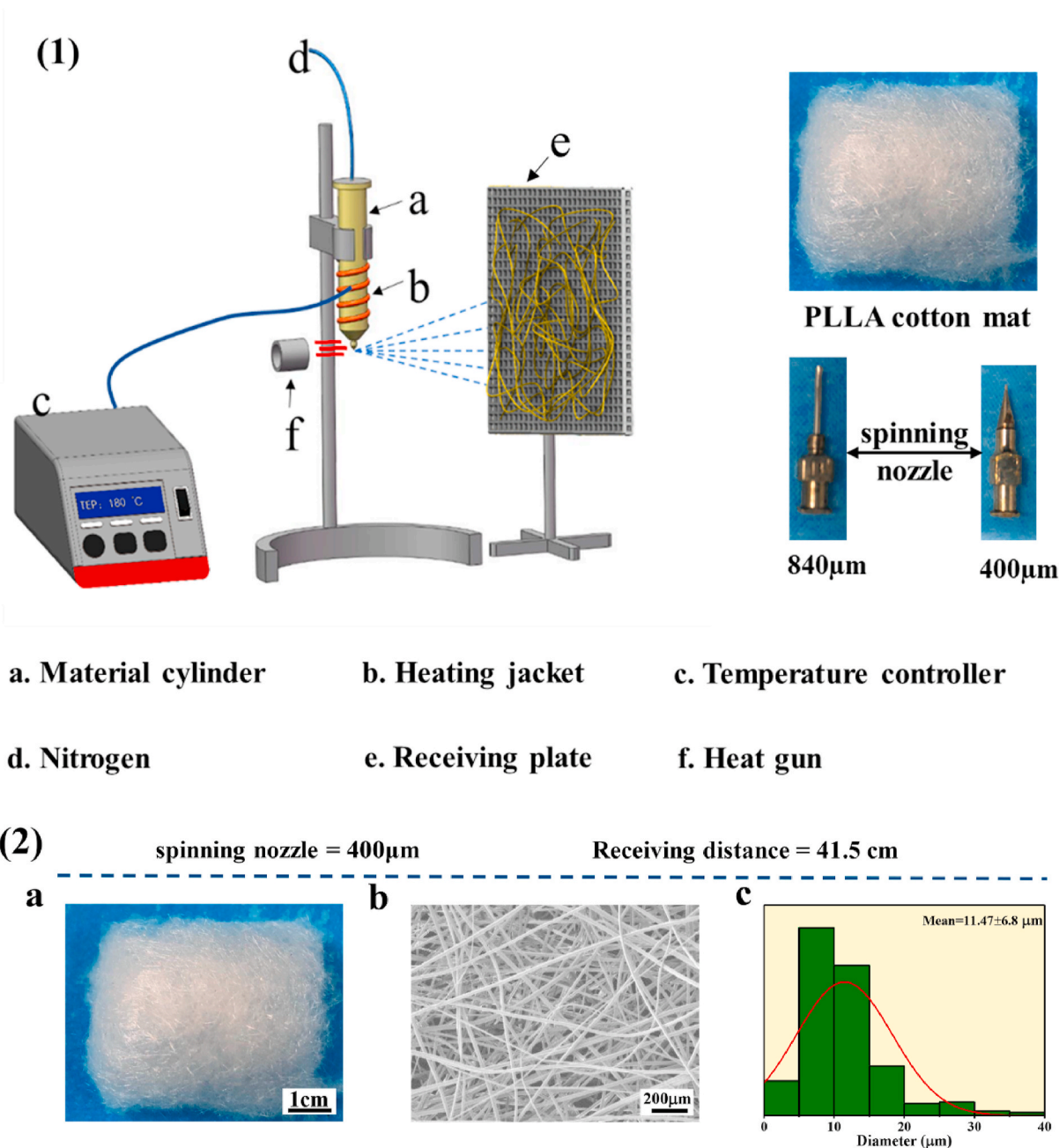
Fig. 1. (1) Melt spinning system. (2) a. Images of PLLA fibrous captured by a digital camera, scale bar = 1 cm. b. SEM micrographs of PLLA fibrous, scale bar = 200 μm. c. The diameter distribution of PLLA fibrous.

and the elemental composition of the samples was determined by energy-dispersive X-ray energy spectrometry (EDX; Philips, XL-30 W/ TMP, Japan). The diameter distribution of the PLLA melt spinning fibre was analysed by NIH ImageJ software (national institutes of health). The mechanical properties of the PLLA fibre were acquired using a universal mechanical testing machine (Instron 1121, UK). The water contact angle was measured by a contact angle system (VCA 2000, AST).

### 2.7. Measurement of absorption rate in vitro

The water absorption rate of samples was measured in PBS (pH 7.4) solution. In brief, the PLLA melt spinning mat and SD/PLLA composites were cut into squares of 3 cm × 3 cm. The mass of each sample was weighed and recorded as m_0. The prepared PBS solution was placed in a constant temperature instrument (37 °C). The samples were immersed in

PBS solution for 1, 3, 5 and 7 min. After the specified times, the samples were removed and held air for 1 min with tweezers to remove the un-absorbed PBS. The samples were weighed again, and their weights were recorded as m_1. Three parallel samples were tested for each sample. Formula (1) W_f is the water absorption rate per square metre, m_0 is the initial weight of the sample and m1 is the weight of the samples after water absorption.

$$\mathrm{wf}(\%) = \frac{m1 - m0}{m0} \times 100\% \tag{1}$$

2.8. Hemolysis ratio

The haemolysis ratio was determined following a previously re-ported method [38]. About 10 mg of sample was immersed into 4.5 mL of normal saline at 37 °C for 24 h to yield the leaching solution.
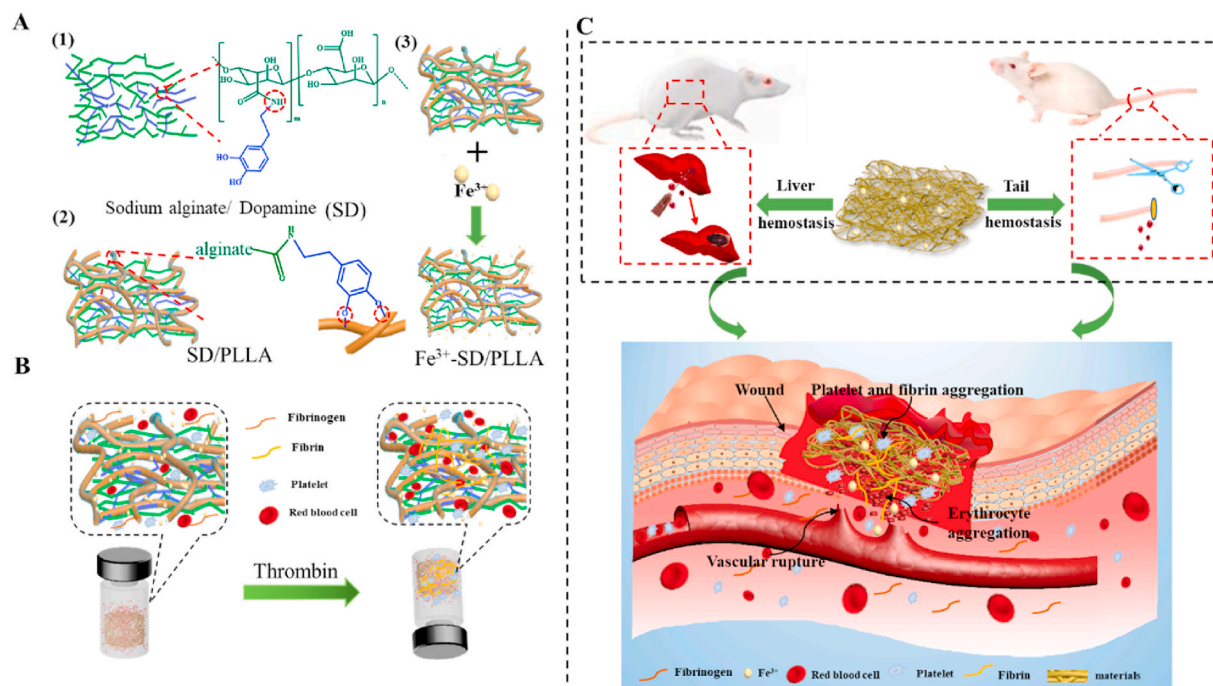
Scheme 1. Hemostatic schematic illustration of nonwoven fibers mat. (A) Chemical structures of three functional components for construction of functional fibers mat. (B) Sketch showing coagulation process in vitro of nonwoven fiber styptic cotton. (C) Nonwoven styptic cotton was used to hemostasis in the liver and tail of rat.
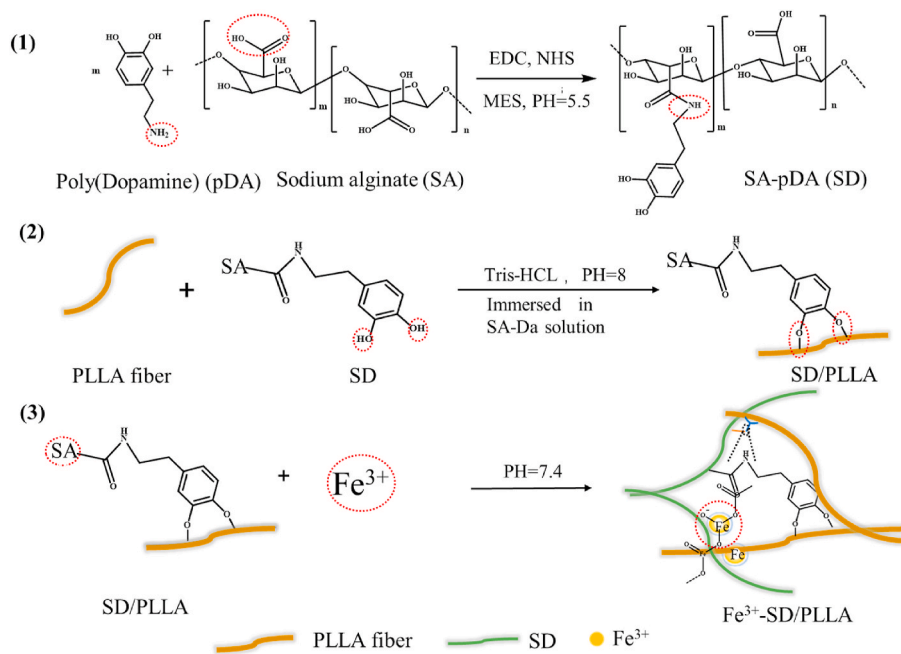
Scheme 2. The specific reaction process of nonwoven fiber styptic cotton.

Subsequently, 125 μL of leaching solution was injected into 875 μL of fresh anticoagulant erythrocyte solution (2%) and fully mixed. The mixed solution was centrifuged (2000 rpm for 10 min) after incubation for 1 h (37 °C). The absorbance of the supernatant was finally measured at 540 nm. Three parallel samples were tested for each sample. The haemolysis ratio was determined as follows:

$$\text{Hemolysis ratio } (\%) = \frac{Bs - Bn}{Bp - Bn} \times 100\% \qquad (2)$$

B_s, B_p, and B_n are the absorbance of the samples, positive control

(Triton X-100, 0.8%) and positive control (normal saline), respectively.

2.9. Antibacterial activity

The antibacterial properties of the material were studied using the method of a previous report [38]. In brief, 8 mL of bacterial suspension (*Escherichia coli* ATCC 8739 and *Staphylococcus aureus* ATCC 29213) in medium (1×10^4 CFU mL^{-1}) was incubated with 20 mg of material for 8 h at 37 °C. The OD at 600 nm of a bacterial culture was then measured. Those without added materials were used as the negative control group.

Three parallel samples were tested for each sample.

In addition, 100 μL of bacterial suspension in sterilised PBS (1×10^4 CFU mL^{-1}) was incubated with sample (0.5 cm planchet on agarose culture plate, five parallel samples) for 24 h at 37 °C. Colony-forming units on the agarose culture plate were observed, and the antimicrobial ring size was measured by Image J. Four parallel samples were tested for each sample.

2.10. In vitro hemostasis performance

The effect of composites on blood clot compared with medical gauze was evaluated according to previous studies [39,40]. In brief, fresh blood (9:1 whole blood to 3.2% sodium citrate) was collected from healthy rabbit (from Liaoning Provincial Laboratory Animal Resources Centre). Blood clot formation was initiated by adding 200 μL of citrated blood to the pre-weighed materials (W$_0$), which were already placed in a 24-well plate at 37 °C. After 1 h of incubation, the sample was rinsed with distilled water three times, and water was carefully dropped into a 24-well plate to avoid blood clot disruption. The blood clot formed was fixed by 37% formaldehyde solution for 10 min. The samples were dried in the oven at 50 °C, and their weight was recorded as (W$_1$). Three parallel samples were tested for each sample. The thrombogenicity of samples was calculated based on the following formula (3):

$$\text{Blood Clot } (\%) = \frac{W1 - W0}{W0} \times 100\% \qquad (3)$$

The platelet and erythrocyte adhesion test was processed based on published methods [5]. In brief, 200 μL of citrated whole rabbit blood was added to a 24-well plate with 5 mg of samples and incubated at 37 °C for 30 min. Subsequently, the non-adhesive blood was rinsed three times with PBS solution and fixed with 2.5% formaldehyde for 3 h. The sample was washed three times with PBS solution to remove formaldehyde, followed by gradient dehydration with 20%, 40%, 60%, 80% and 100% aqueous ethanol and dried at 30 °C. The adherence of RBCs on the sample surface was observed by SEM after the samples were coated with gold.

The whole blood coagulation ability of composites was measured following a method adopted from Shih et al. [41] In brief, 5 mg samples were placed in a 24-well plate at room temperature. Subsequently, 200 μL of rabbit blood was dropped slowly. The reaction was triggered by adding 10 μL of CaCl$_2$ (0.2 M) solution. The reaction was incubated for approximately 30 min with shaking 30 rpm at 37 °C, and unstable blood clots were dissolved by rinsing with distilled water three times. The absorbance values of the suspension at 544 nm [42] were measured by using a microplate reader (Infinite M200; Tecan, Switzerland). Three parallel samples were made for each sample.

About 10 mg of the sample was weighed and transferred into a 2 mL disposable plastic tube that was placed in a 37 °C incubator for about 10 min. Fresh blood was obtained from the rabbit with a medical vacuum collective tube containing sodium citrate anticoagulant and placed in the 37 °C incubator for about 10 min. About 200 μL of the blood was added into the 2 mL sample tube, and the time was recorded after the addition of CaCl$_2$ solution (10 μL, 0.1 M). The disposable plastic tube was inverted every 10 s. When the blood was completely stagnant, the time was recorded. Every sample was tested three times.

2.11. Cytocompatibility

For the following experiments, the materials were placed into a 24-well plate and sterilization by UV-light irradiation for 3 h. Subsequently, 2×10^4 cells NIH-3T3 were seeded into the 24-well culture plate containing materials and cultured using DMEM in a humidified atmosphere of 95% air and 5% CO$_2$ at 37 °C. The culture medium was changed every 2 days. Cell viability was measured by CCK-8. After the fibroblasts were cultured on different kinds of materials for 1, 3 and 7 days, CCK-8 solution (100 μL/mL) was added to each well. The cells

were continually cultured for another 2 h, and 150 μL of the reaction solution was transferred into a new 96-well plate. Three parallel samples were made for each sample.

Cell morphology was investigated by fluorescence microscopy after 2×10^4 cells were seeded in 24-well culture plate containing materials that were sterilised for 3 days using DMEM. The culture medium was changed after 2 days. After 3 days, DMEM was removed from the original culture wells, rinsed with PBS (pH 7.4) solution for three times and stained with Calcein-AM (Aladdin, China) for 10 min at 37 °C. Subsequently, the samples were rinsed three times with PBS. Cell morphology was observed using an Axio Imager A2 (Zeiss, Germany) fluorescence microscope.

2.12. Experiment animals

We used 10–12 weeks old male BALA/c mice to study in vivo hemostatic performance and 6 weeks old male SD rat to study tissue compatibility of materials in this research. The animal experiments were carried out according to the NIH Guide for the Care and Use of Laboratory Animals, provided by Jilin University, Changchun. All mice were fed cages in the animal facility for at least 1 week for acclimation prior to experimental use. We used CO$_2$ inhalation followed by cervical dislocation to euthanize the animals.

2.12.1. In vivo hemostatic performance

The samples were cut into squares (1 × 1 cm^2). Before the experiment, samples were sterilised by UV-light irradiation for 3 h. The liver and tail injury models (BALA/c male rat, 21–23 g, 10–12 weeks old) were used to investigate the hemostatic properties of the material in accordance with a previously reported method [43,44]. Briefly, the mice were anesthetized and fixed on the surgical corkboard, which was disinfected in abdomen with Iodine and 75% alcohol. The abdominal skin was cut and the hepatic anterior was exposed. The blood and tissue fluid of incision site was cleaned by medical sterile gauze. Then the pre-weighted (W$_1$) filter paper was placed under hepatic. A wound was made by 26 G (outer diameter: 460 μm) sterile needles so that the blood out from the wound rapidly. The hemostatic cotton was put on the bleeding until the bleeding stopped. Finally, the blood loss time (s) were recorded and the filter paper was weighted (W$_2$). Three parallel samples were made for each sample.

$$\text{Blood loss } (g) = W2 - W1 \qquad (4)$$

2.12.2. Histocompatibility

Muscles of the rat back implantation model were used to study tissue compatibility (SD rat, 200 g, 6 weeks, male rats). Male were anesthetized and 2 mg (0.5 cm diameter disc) of sample was inserted into the back muscles of the rats (n = 5). At given time intervals (days 0, 7 and 14 days), the rat was sacrificed to isolate materials and surrounding tissues and fixed with glutaraldehyde (4%). The fixed tissues were embedded in paraffin to cut into sections. After gradient dehydration, tissue sections were stained with H&E and tissue compatibility was observed.

2.13. Statistical analyses

All data were analysed through Origin 8.0 (Origin Lab Corporation, USA) and shown as the mean ±standard deviation. One-way analysis of variance was used for statistical comparison. $p < 0.05$ was considered statistically significant.

3. Results and discussion

3.1. Characterization

3.1.1. Morphology and diameter distribution analysis of PLLA fibre
Fig. 1(2) and Fig.S2 showed the PLLA melt spinning mat exhibited a

cotton-like bouffant state with massive un-melted PLLA polymers on the fiber surface in the groups of 33.7 cm and 44.8 cm and less bulk polymer on the fibre surface was observed in the group 41.5 cm when the 840 μm spinneret were used. While, there was no bulk PLLA polymer on the fibre surface and the fibres were uniform when the receiving distance was 41.5 cm and 400 μm spinneret was used. The morphology and diameter distribution of PLLA fibre was characterized by SEM and analysed by image J software. An interconnected mesh structure was observed with the fibre surface smooth and the size distribution was mainly from 5 to 15 μm in group of 41.5 cm when the spinneret was 400 μm (Fig. 1(2c)). In the groups of 33.7 cm, 41.5 cm and 44.8 cm (840 μm), the morphology of PLLA fibre was similar that of the group of 41.5 cm (400 μm) showing interconnected structure. The diameter of PLLA fibre decreased with the receiving distance increased when 840 μm spinneret was used.

From the above results PLLA fibre mat was prepared using different spinning spinneret and receiving distance, it was found that the fibre surface had some un-melted polymer when the spinneret was 840 μm. However, when the spinneret was 400 μm, the un-melted polymer on fibre surface was disappeared. It might be attributed to the temperature of the 400 μm spinneret was kept at 190 °C for both the core and sheath [45]. Therefore, the polymer of PLLA was melted uniformly and the melt flow rate of PLLA achieves stability [46,47]. However, the melt of PLLA polymer would be cooled agglomeration as it flow to the end of the 840 μm spinneret due to its temperature of the 840 μm spinneret lower glass conversion temperature of PLLA polymer [48]. We can observe that the diameter of fibre became tiny with receiving distance increased when 840 μm spinneret was used. The reason might be that the stretching time of fiber increased at the high flux hot wind environment as the receiving distance increased. In addition, under the same receiving distance, the diameter of fibre made by 400 μm spinneret was smaller than that of fibre made by 840 μm spinneret. It might be related to the orifice of spinneret and the orifice of 400 μm spinneret was smaller than the 840 μm spinneret.

3.1.2. Mechanical property of PLLA fibre

The mechanical properties of a scaffold used to filling deep wound is important paremeters [49]. The tensile strength of PLLA fibre made in different preparation conditions displayed in Fig S3. In the groups of 33.7 cm, 41.5 cm and 44.8 cm (840 μm), the tensile strength of PLLA fibres was 7.0, 3.8 and 6.4 Mpa, respectively. At the same time, the breaking strain was 8.3%, 12.0% and 7.9%, respectively. When the PLLA fibre made by 400 μm spinneret and the receiving distance is the same (41.5 cm), the tensile strength and breaking strain were reduced to 1.5 Mpa and 8.3%. The diameter distribution measurements showed that the diameter of fibre influence tensile strength of fibre. These results are consistent with previous report, suggesting that the mechanical properties were found to be dependent on fibre diameter [50].

3.1.3. Chemical characterization

The chemical structures of SD/PLLA and Fe^{3+}-0.5SD/PLLA composites were characterized by FTIR. As shown in Fig. S4, a strong single absorption peak was observed in the PLLA absorption band at 1749 cm^{-1}, which belonged to the C=O stretching vibration absorption of PLLA. The absorption peak at 1182 cm^{-1} was due to the C–O–C asymmetric stretching vibration or the out-of-plane bending vibration of -CH3. The absorption band at 1087 cm^{-1} was attributed to C–O–C symmetric stretching vibration [51,52]. In the spectrum of the SD/PLLA composite, the broad absorption peak at 3000–3600 cm^{-1} was due to the symmetric stretching vibration of –OH and –NH_2 [53]; –OH was derived from SA and pDA, while –NH_2 belonged to pDA. The typical absorption peaks of SA observed at 1600 and 1415 cm^{-1} were assigned to the stretching vibration absorption peaks of –COO– [54]. The peak strength increased with the increase in the SD concentration. The primary changes for SD were the shifts in amide. To our satisfaction, the –C=O stretching vibration, –CONH– bond vibration and C–N bond

vibration bands were observed at 1602.7, 1546.8 and 1278.7 cm^{-1}, respectively. In Fig. 2(2), the absorption peak strength of –COO– at 1600 and 1415 cm^{-1} and the absorption peak strength of –OH at 3000–3600 cm^{-1} were reduced when Fe^{3+} was introduced compared with 0.5SD/PLLA. This reduction was due to the chelation of Fe^{3+} with –COO– and –OH [55,56]. At the same time, a weak absorption peak appears around 600-700 cm^{-1} on 5Fe^{3+}-&, 10Fe^{3+}-& and 20Fe^{3+}-& absorption curve, which show that there is iron oxide phases formation [57]. The results indicated that the amidation reaction successfully occurred between the carboxyl of SA and the amino of pDA and the chelation was formed among Fe^{3+}, COO- and –OH.

Fig. 2 (3) and Fig S5 showed the wide scan spectra of PLLA, pDA and 0.5 SD/PLLA. Two peaks corresponding to C1s (285 eV) and O1s (532 eV) were observed in all the samples. Additionally, a distinct N1s peak at 400 eV was observed in pDA and 0.5 SD/PLLA samples. Fig. S5 (a) showed that a symmetrical single peak was observed at 406.6 eV on the spectrum of pDA belonging to C–NH_2 on pDA. When the absorption band of pDA was compared with the absorption band of 0.5 SD/PLLA (Fig. S5 (b)), two peaks appeared at 401.3 and 399.5 eV, corresponding to N–C=O and N–C- of 0.5 SD/PLLA, respectively [58]. The data further demonstrated that the formation of amide bonds between SA and pDA.

3.1.4. Surface morphology of composite

As shown in Scheme 2(1, 2), the SD composite was formed by amidation and then modified (0.1%, 0.3% and 0.5%; w/V%) onto the surface of hydrophobic PLLA fibre through DA, which was inspired by mussel byssus [59]. To further improve hemostatic performance, Fe^{3+} (5, 10 and 20; mM) was introduced into the 0.5SD/PLLA composite, as shown in Scheme 2(3). Compared with PLLA fibre, the surface colour of the fiber deepened when the SD polymer was immobilized on the surface of the PLLA fibre, and the colour of the composite further deepened with the increase of Fe^{3+} concentration (Fig. 2(1a)). Compared with PLLA fiber, there were microfibers on the surface of the fibre composite. Furthermore, the white reticular material on the surface of the PLLA fibre became denser, and the clearance between the fibres became smaller with the increase of SD concentration (Fig. S6(1b)). Meanwhile, the surface of the fibers also had a layer of white material (Fig. 2(1b)). The white reticulated was disappeared but deposited on the surface of the fibre, which may be caused by a chemical reaction between SD and Fe^{3+}.

The concentration of Fe^{3+} released in PBS on Fe^{3+}-0.5SD/PLLA composite was measured by ICP and the elemental distribution of was observed using EDX mapping. From the result of Table S2, we find that the Fe^{3+} content is being increase in PBS solution before 4 min for 5Fe^{3+}-0.5SD/PLLA, 10Fe^{3+}-0.5SD/PLLA and 20Fe^{3+}-0.5SD/PLLA composites. The Fe^{3+} content in PBS solution for 20Fe^{3+}-0.5SD/PLLA material is still increasing at 8 min compared at 2 min and 4 min. However, the Fe^{3+} content for 5Fe^{3+}-0.5SD/PLLA and 10Fe^{3+}-0.5SD/PLLA composites become decrease in PBS solution at 8 min compared at 2 min and 4 min. The above result indicated that more Fe^{3+} carried on 20Fe^{3+}-0.5SD/PLLA material and the Fe^{3+} can be continuously released into PBS solution. The Fe^{3+} ions could hydrolysis in water solution and generate precipitation [60], which might be the reason for the decrease of Fe^{3+} content in the PBS solution for 5Fe^{3+}-0.5SD/PLLA and 10Fe^{3+}-0.5SD/PLLA material at 8 min. In addition, we speculated that there are no excess Fe^{3+} ions released on 5Fe^{3+}-0.5SD/PLLA and 10Fe^{3+}-0.5SD/PLLA composite. EDX mapping over a representative 20 Fe^{3+}-0.5SD/PLLA composite in Fig. 2(1c) shown a homogeneous distribution of the elemental C, N, O, Na and Fe elements.

3.1.5. Water contact angle analysis

After confirming the immobilized of SD on the surface of PLLA fibre. The static hydrophilic measurements of samples are shown in Fig. 3(1). The water contact angle of the PLLA fibrous was 116°. However, when 0.1% SD was modified on the PLLA fibre mat, the water contact angle of the 0.1SD/PLLA composite declined rapidly from 116° to 0°, which
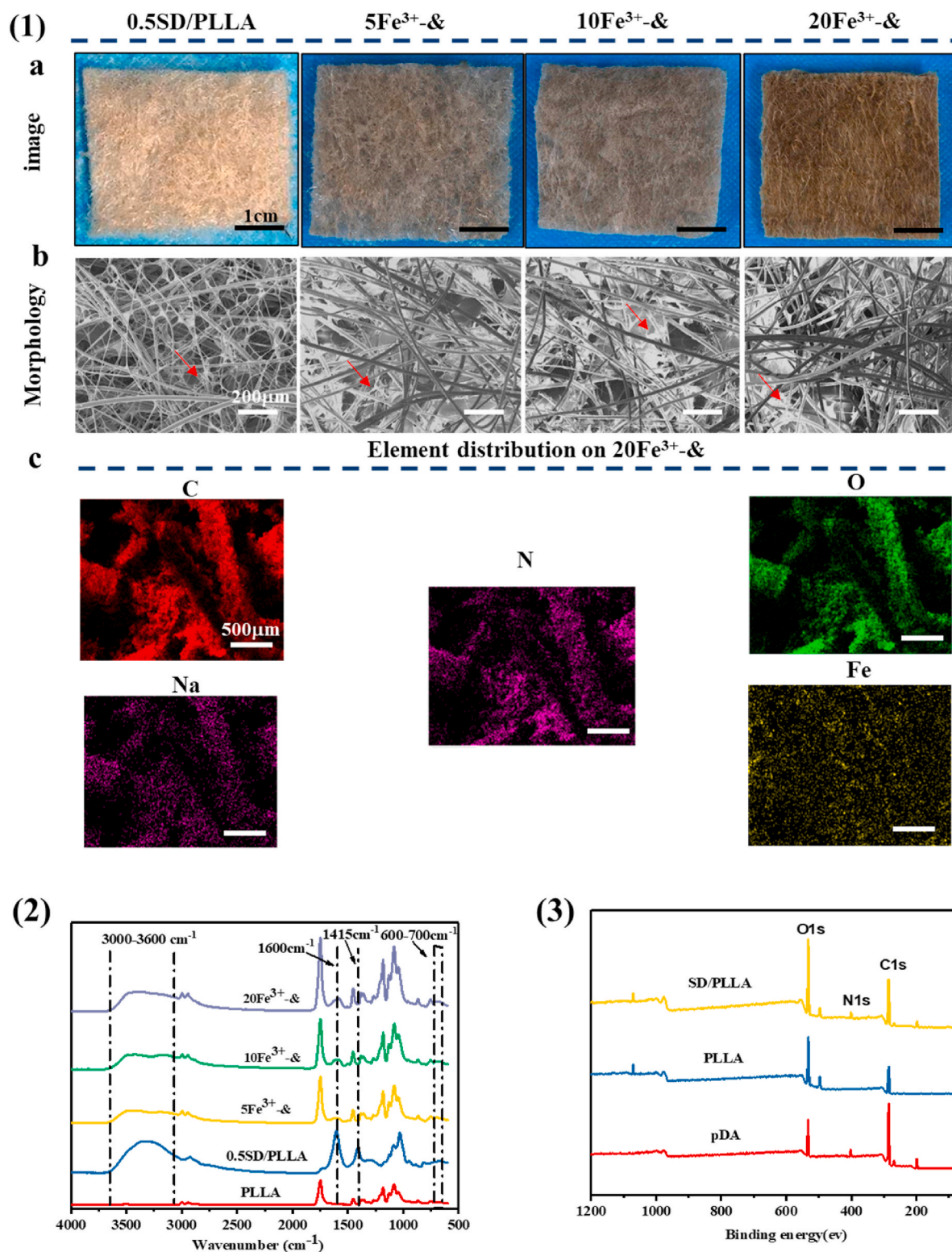
Fig. 2. (1) a. Images of composite materials captured by a digital camera, scale bar = 1 cm. b. SEM of composite materials, scale bar = 200 μm. c. Element distribution on 20 Fe^{3+}-& composite materials, scale bar = 500 μm. (2). FT-IR of samples. (3). XPS of PLLA fibrous, pDA and 0.5 SD/PLLA. & representative 0.5SD/PLLA.

illustrated that SD greatly improved the hydrophilic property of the fibre surface. This SD/PLLA melt spinning fibrous mat composite demonstrated high hydrophilicity and wetting ability with the increase in the SD (0.1, 0.3 and 0.5, w/V%) concentration.

Previous research has reported that the PLLA fibrous had strong hydrophobicity [51]. SINGH et al. had reported that SA was used as a hydrophilic coating to enhance the water absorption ability [61]. The sharp increase in surface hydrophilicity of the composite was possibly due to the presence of the hydroxyl group on pDA and SA and the carboxyl group on SA outwards to the hydrophilic environment
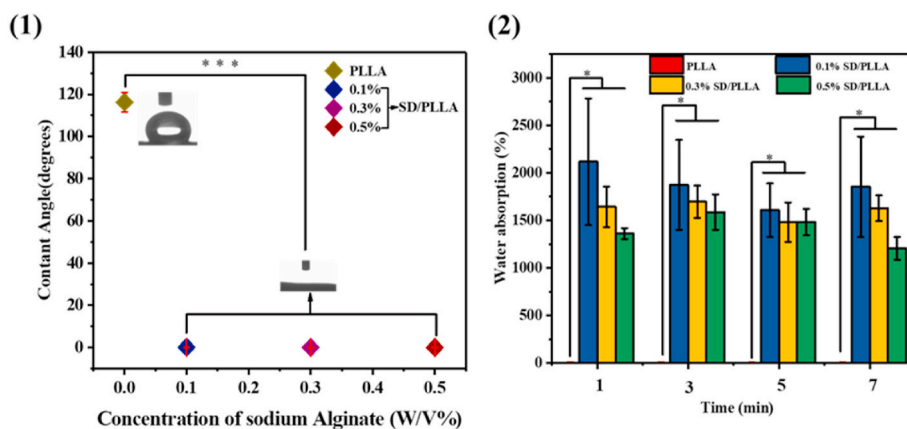
Fig. 3. (1) Contact angle of PLLA fibrous and SD/PLLA composite. (2) PBS absorption rates of PLLA fibrous and SD/PLLA composite. * present a significantly difference about PLLA fiber and SD/PLLA composite with different concentration of SD at $P < 0.05$, respectively.

(hydroxyl and carboxyl groups have hydrophilicity) as manifested. The decrease in the water contact angle led to higher wetting ability on the surface of the fibrous mat composite.

3.1.6. PBS absorption rates analysis

As illustrated in Fig. 3(2), the PBS absorption property of the PLLA fibrous presented nearly no water absorption property compared with that of the SD/PLLA composite. However, the PBS absorption rates of the PLLA fibrous were greatly improved after the modification of the SD composite on the fibre surface. The maximum PBS absorption rates of SD/PLLA reached 2116% after the 0.1% SD polymer was modified on the PLA fibre mat. The PBS absorption rates of the SD/PLLA composite decreased with the increase in the SD composite concentration at the same time frame. This phenomenon may be due to the slight decrease in the porosity between fibres with the introduction of SD polymer into the PLLA fibrous, thereby preventing water entering the composite. Such a result could also be explained by the reaction between –COOH of alginate and –NH$_2$ of dopamine groups. Hence, these groups could not form hydrogen bonds with water molecules [62]. Under the modification of SD at the same concentration, the PBS absorption rate of the fibrous mat hardly changed significantly in different time periods. The hydrophilicity of the fibre surface was greatly improved after the modification of the SD composite, and the fibrous mat composite quickly reached saturation state after immersed into PBS. This state is conductive to the rapid absorption of wound exudate and acceleration of hemostasis. Additionally, the unreacted carboxyl groups on the alginate and the unreacted hydroxyl and amino groups on dopamine on the surface of the fibre material rapidly formed hydrogen bonds with the water molecules to keep water inside the fibre.

3.2. In vitro hemostasis property analysis

3.2.1. Whole blood clotting

The hemostatic property of melt spinning hemostatic fibrous mat was studied by calculating the percentage of blood clot formed. The results in Fig. S6 (2) indicated that more blood clots formed on the surface of SD/PLLA composite than on the medical gauze. The blood clot ratio could up to 75% when the concentration of SD was 0.5%. As shown Fig. 4 (2), the blood clot ratio was 162%, 183% and 213% for 5Fe^{3+}-0.5SD/PLLA, 10Fe^{3+}-0.5SD/PLLA and 20Fe^{3+}-0.5SD/PLLA composites. The result showed that blood clot ratio increased with Fe^{3+} content increase on 0.5SD/PLLA material. It increased nearly threefold compared with the 0.5SD/PLLA composite when the Fe^{3+} concentration was 20 mM. Meanwhile, Fig. S6 (1a) and Fig. 4 (1a) also confirmed the results of the blood clot experiment. We find that trivalent iron indeed played a vital role in blood clot formation. The results corroborate the finding of the previous work [63,64]. It may be due to dense matted

deposits and red blood cell aggregates (Scheme 1 B) be induced in normal blood by the additions of trivalent iron. The Fe^{3+} can causes major oxidative stress through free radical generation, which leads to lipid peroxidation and destruction of endothelial cells and leading to occlusive thrombus formation.

To verify the above results, the blood clotting behaviour was further investigated by determining haemoglobin absorbance at 544 nm (OD$_{544}$). OD$_{544}$ was used as a coagulation activity index. Lower haemoglobin absorbance at 544 nm value indicates a better blood clotting ability. As shown in Fig. S6(4), the OD$_{544}$ values of medical gauze was 1.770 ± 0.012. The haemoglobin absorbance on 0.1SD/PLLA, 0.3SD/PLLA and 0.5SD/PLLA was 0.016 ± 0.006, 0.400 ± 0.003 and 0.300 ± 0.014, respectively. However, the OD$_{544}$ values of Fe^{3+}-0.5SD/PLLA, which had much lower absorbance of haemoglobin than medical gauze and 0.5SD/PLLA composite. The absorption capacity at 544 nm for 5Fe^{3+}-0.5SD/PLLA, 10Fe^{3+}-0.5SD/PLLA and 20Fe^{3+}-0.5SD/PLLA were 0.230 ± 0.002, 0.100 ± 0.003 and 0.080 ± 0.003, respectively. These results indicated that the concentration of SD and Fe^{3+} had an influence on the hemostatic property. The hemostatic mechanism of SD/PLLA was that the strong hydrophilicity and PBS absorption ability promote platelet adhesion, clotting factors binding and lead to clot formation rapidly [65], due to the blood clot was aggregate of platelet, erythrocytes and fibrin. Furthermore, the Fe^{3+} can promote the formation of thrombosis [31]. The trivalent ions can react with blood form coagulum of blood proteins. The proteins agglutinate to form plugs that occlude the capillary orifices. Thus, the trivalent ions effective hemostasis through a chemical reaction with blood [66,67]. Specifically, free Fe^{3+} functioned as a thrombogenic agent via generation of hydroxyl radicals, which modified fibrinogen molecules to make them resistant to fibrinolysis and stimulated the blood coagulation cascade [63]. Therefore, the blood clot formed rapidly under the synergistic effects of Fe^{3+} and SD.

3.2.2. Hemostatic time study

Hemostatic time was the most direct method to evaluate the hemostatic ability of materials. From the results shown in Fig. S6(3), the hemostasis time of medical gauze 0.1SD/PLLA, 0.3SD/PLLA and 0.5SD/PLLA were 417 ± 19, 353 ± 6, 201 ± 8 and 120 ± 6 s, respectively. Fig. 4 (5) shows the hemostasis times of 5Fe^{3+}-0.5SD/PLLA, 10Fe^{3+}-0.5SD/PLLA and 20Fe^{3+}-0.5SD/PLLA were 119 ± 6, 96 ± 15 and 48 ± 28 s, respectively. The hemostatic time shortened from 417 s to 120 s when 0.5SD/PLLA was used and the hemostatic property was improved with SD concentration increased. The reason might be that the hydrophilicity allowed the material to absorb water at a rapid rate, which made its initial blood absorption time shorten [68]; hence, the material could control bleeding quickly and effectively. In addition, the hemostatic time was much faster than those SD/PLLA composite when Fe^{3+} added
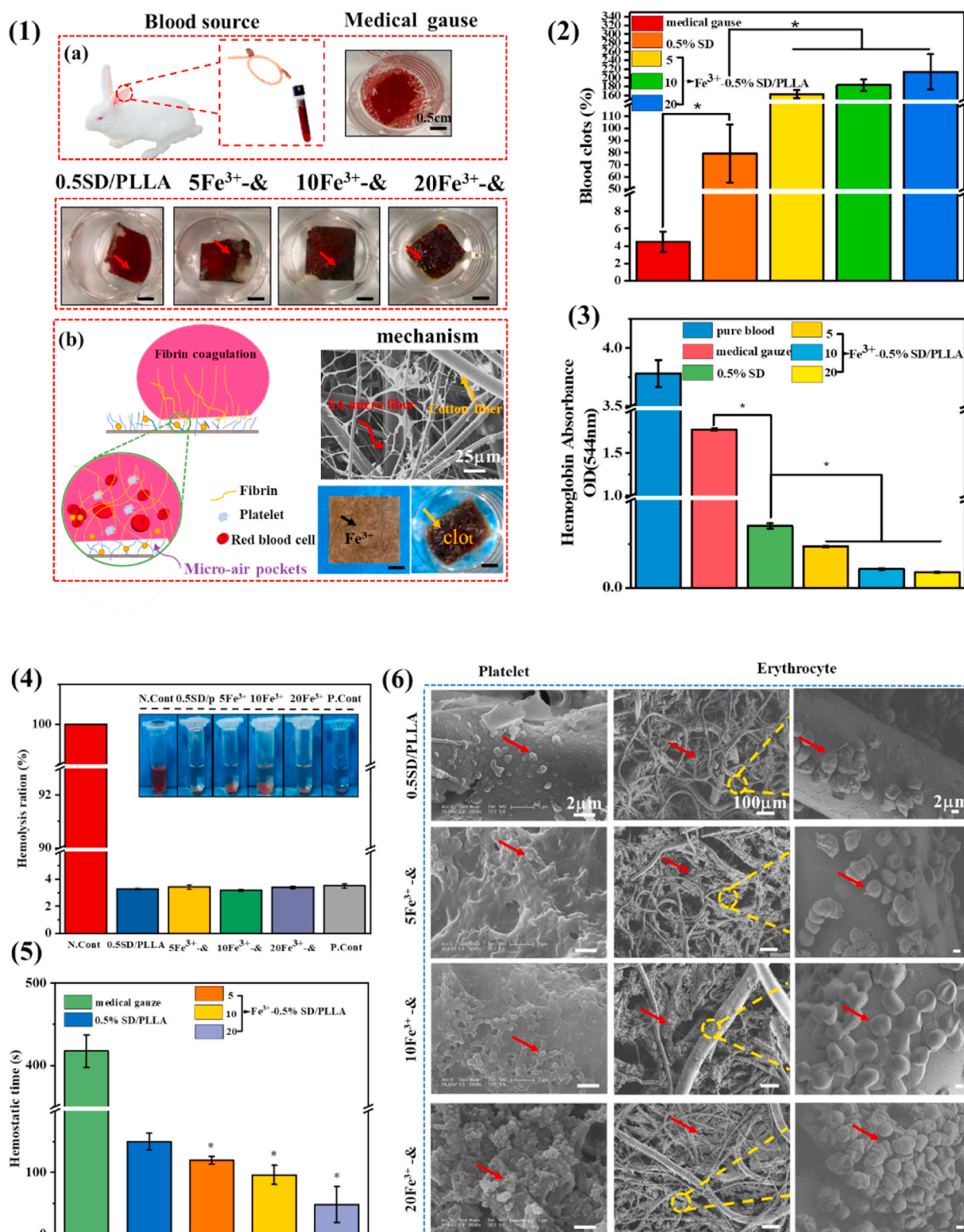
Fig. 4. (1) Blood clot on materials captured by a digital camera (a), scale bar = 0.5 cm. Mechanism of materials for hemostasis (b). (2) Quantitative results of blood clots formation to the different material surface. (3) The absorbance of hemoglobin in pure blood and uncoagulated blood on the materials. (4) The hemolysis ration of composite material. (5) the hemostatic time of the different material. (6) SEM micrographs of platelet and erythrocyte agglutination and adhesion on the surface of materials. * present a significantly difference about different materials at $P < 0.05$. & representative 0.5SD/PLLA.

to 0.5SD/PLLA composite. There was carboxyl on SA and phenolic hydroxyl on DA, which would form hydrogen between water molecules in the blood. What's more, Emiliya M et al. [69] reported that hydrogen and electrostatic bonds take part in the formation of the fibrin aggregate.

Moreover, the formation of the fibrin aggregate could be accelerant by substance carrying a positive charge. The aggregation of fibrin monomer was an important stage in hemostatic process.

3.2.3. Platelet and erythrocytes adhesion

The morphology of blood clot formed on the surface of materials was observed by SEM. As shown in Fig. S6(5), the numerous platelets that adhered on the surface of SD/PLLA materials increased as the SD concentration increased. There was a small increase in the adhesion of platelets after Fe^{3+} addition but it was independent of the Fe^{3+} concentration (Fig. 4(6)). These results were due to the fact that the material morphology was found to have a greater effect on platelet adhesion and activation [70]. The mechanism of blood clot formation is shown in Fig. 4(1b). With the increase in the SD concentration, more nanofibers of SD formed on the surface of the PLLA fibre (Fig. S4(1b)) and the nanofibers were reported to contribute to platelet adhesion [71]. By contrast, a large number of erythrocytes gathered on the surface of Fe^{3+}-0.5SD/PLLA materials, and the number of erythrocytes increased with the Fe^{3+} concentration. In previous report that the iron-induced modification of fibrinogen molecules is responsible for enhanced interaction with erythrocytes and lead to erythrocytes gathered [63]. The experiment results (Fig. 4(1a)) also confirmed the above mechanism that the amount of blood clot formation increased with the increase in Fe^{3+} concentration.

3.3. In vivo hemostatic performance

3.3.1. The liver hemostasis property of rat

Fe^{3+}- 0.5SD/PLLA styptic cotton with different concentration of Fe^{3+} had been proved to exhibit preferable hemostatic properties through in vitro hemostatic experience, so its hemostatic behaviour was further demonstrated by the liver hemostasis model and tail rupture of rat (Scheme 1 C). PLLA fibrous and 0.5SD/PLLA was selected as the control groups. However, bleeding from the rat liver was affected by many

factors, such as the size of the liver and constitution of the rat. To minimise experimental error, three rats for each material were used. A pinhole was made on the rat liver by using a 25 G sterile needle (0.26 mm). The hemostasis steps of rat liver are shown in Fig. 5(1a). After liver damage was initiated, the material was covered until the bleeding stopped. The results of hemostasis are summarised in Fig. 4(3) and Fig. 4 (4). The hemostatic time of control was 121 s, and the amount of blood loss reached 0.33 ± 0.17 g. The hemostatic time of 0.5SD/PLLA (55 ± 6.24 s) was less than that of the PLLA fibrous (63 ± 2 s), and the blood loss showed no noticeable change. After adding Fe^{3+} on 0.5SD/PLLA, the hemostasis time was further reduced, and the shortest hemostasis time reached 23.33 ± 3.51 s at an Fe^{3+} concentration of 20 mM. However, blood loss slightly decreased, and the blood loss amounts were about 0.125 ± 0.020, 0.070 ± 0.053 and 0.097 ± 0.030 g for $5Fe^{3+}$-0.5SD/PLLA, $10Fe^{3+}$-0.5SD/PLLA and $20Fe^{3+}$-0.5SD/PLLA, respectively. In the hemostasis process, the PLLA fibrous applied certain pressure on the wound and resulted in less blood flow than the control group. By contrast, the composite material could absorb the outgoing blood and cause the accumulated blood to form a thrombus; large quantities of erythrocytes and platelets gathered on the surface of the wound to form a physical barrier [38]. Furthermore, Fe^{3+} resists fibrinolysis and triggers a coagulation cascade that speeds haemostasis. The synergistic effect of the above properties makes styptic cotton had better hemostasis effect for incompressible wound.

3.3.2. The tail hemostasis property of rat

The hemostatic time was further quantified in the rat tail amputation model (Fig. 5(1b)). The results are shown in Fig. 5(2). The hemostasis times were 118 ± 3 and 87 ± 6 s for the control and PLLA fibre mat, respectively. The hemostasis time decrease to 56 ± 11 s when 0.5SD was
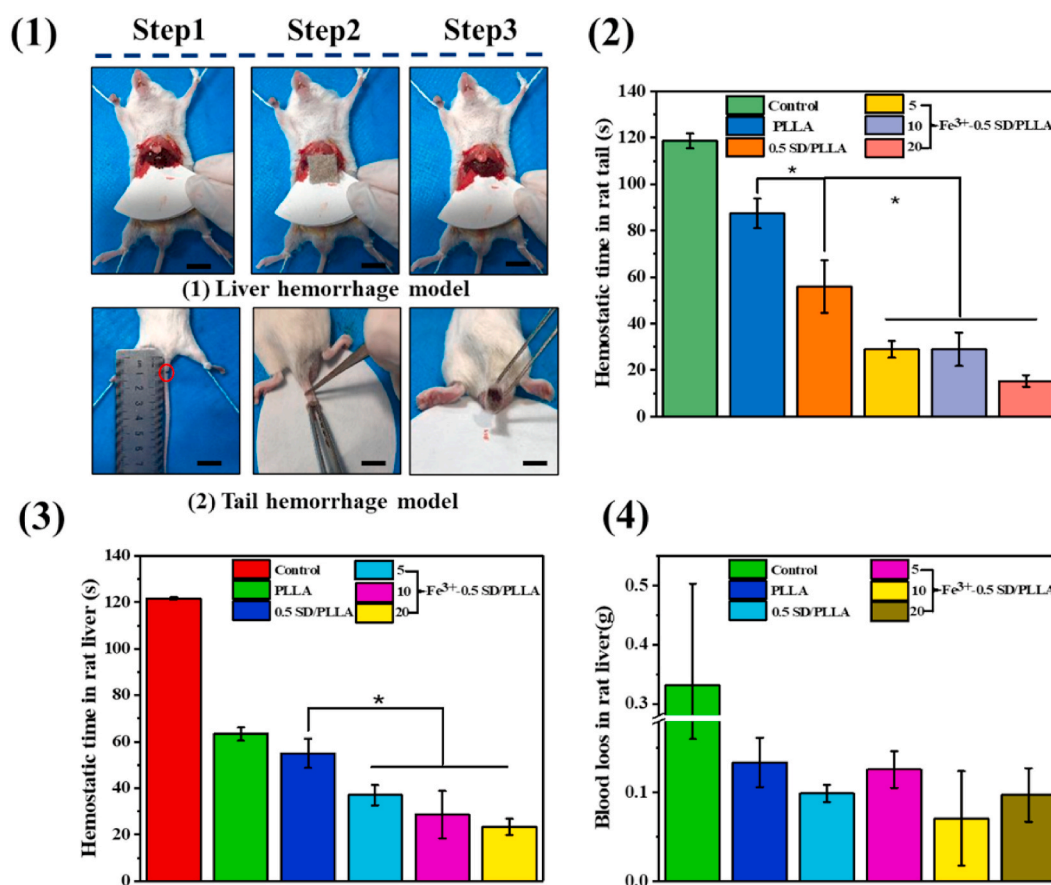

Fig. 5. (1) Photographs of in vivo hemostasis by nonwoven fiber styptic cotton on rat liver and rat tail as wound model, scale bar = 0.5 cm. Hemostatic capability of the styptic cotton: (2) hemostatic time in rat tail. (3) hemostatic time in rat liver (4) blood loos in rat liver. * present a significantly difference at $P < 0.05$.

combine to the surface of PLLA fiber. Specifically, the Fe^{3+}-SD/PLLA material showed significant hemostasis property and different with 0.5SD/PLLA ($p < 0.05$). The hemostasis time was 15 ± 2 s when the Fe^{3+} concentration was 20 mM. Both in the liver and tail of rats, the 20Fe^{3+}-0.5SD/PLLA showed excellent hemostatic performance. In addition, as an ideal hemostatic material, it should exhibit blood compatibility, cytocompatibility and excellent antibacterial property.

3.4. Cytocompatibility, hemocompatibility and antibacterial activity

3.4.1. Cytocompatibility

As an ideal hemostatic material, materials with good cytocompatibility are extremely important to the human body. As shown in Fig. 6(1), no obvious differences in cell viability were found among medical gauze and other materials at day 1, and the cell activity of the material was higher than that of medical gauze at 3 days. However, at 7 days, there was a slight decrease in cell activity of Fe^{3+}-0.5SD/PLLA than that of medical gauze, and the cell viability value was 78%. Furthermore, the morphology of NIH-3T3 cells grown on materials at 3 days was observed by using a fluorescence microscope after Calcein-AM live cell staining and nuclear staining with DAPI. As shown in Fig. 6(2), all NIH-3T3 mouse fibroblasts exhibited excellent cell spreading pattern in medical gauze and all materials, and a large number of cells grew in the material's surface as revealed by DAPI staining. These results indicated that the 0.5SD/PLLA and Fe^{3+}-0.5SD/PLLA materials exhibited good cytocompatibility.

3.4.2. Hemocompatibility

Hemocompatibility is an important indicator for hemostatic material. As shown in the insets of Fig. 4(4), after blood cells were co-cultured with material suspension, the colour of the obtained supernatant was

slightly yellow similar to the negative control group (PBS) and different from the positive control group (bright red). Furthermore, all samples revealed a low haemolysis ratio (<4%), which met international standards [9]. The above results indicated that styptic cotton featured good hemocompatibility.

3.4.3. Antibacterial activity

During haemostasis, bacterial infection poses a threat to human life [72]. Therefore, antimicrobial properties are important for hemostatic materials. The OD value (600 nm) was used as a bacterial activity index. When the bacteria had a low OD value, then the materials had high antibacterial ability. The results of the quantitative analysis of antibacterial properties of materials for *Escherichia coli* and *Staphylococcus aureus are* shown in Fig. 6(3) and Fig. 6(4), respectively. The OD values of 0.5SD/PLLA were 0.85 ± 0.053 and 0.69 ± 0.017 for *E. coli* and *S. aureus,* respectively. The OD values of 20Fe^{3+}-0.5SD/PLLA were 0.66 ± 0.03 and 0.34 ± 0.08 for *E. coli* and *S. aureus* respectively. From Fig. 6 (3) and Fig. 6(4), we find that the OD values of *E. coli* and *S. aureus* decreased when adding Fe^{3+} on 0.5SD/PLLA material, and the survival rate of the bacteria had slight decrease with the increase in the Fe^{3+} concentration. As shown in Fig. S4, there was less bacterial growth around the material. Fig. 6(5) shown that the quantitative analysis results of antibacterial ring size of 0.5SD/PLLA were 21.2 ± 1.1 and 24.24 ± 4.9 mm for *E. coli* and *S. aureus,* respectively. When the concentration of Fe^{3+} was 20 mM, the antibacterial ring size of *E. coli* and *S. aureus* were 38.3 ± 1.7 and 42.5 ± 2.5 mm, respectively. While, the Fe^{3+} exhibit slight effect for the size of antibacterial ring size for both *E. coli* and S. aureu with the increase in the Fe^{3+} concentration. The results of quantitative analysis of antibacterial ring size were consistent with the findings in Fig. S7. The above results indicating that the 20Fe^{3+}-0.5SD/PLLA exhibit better antibacterial than other group
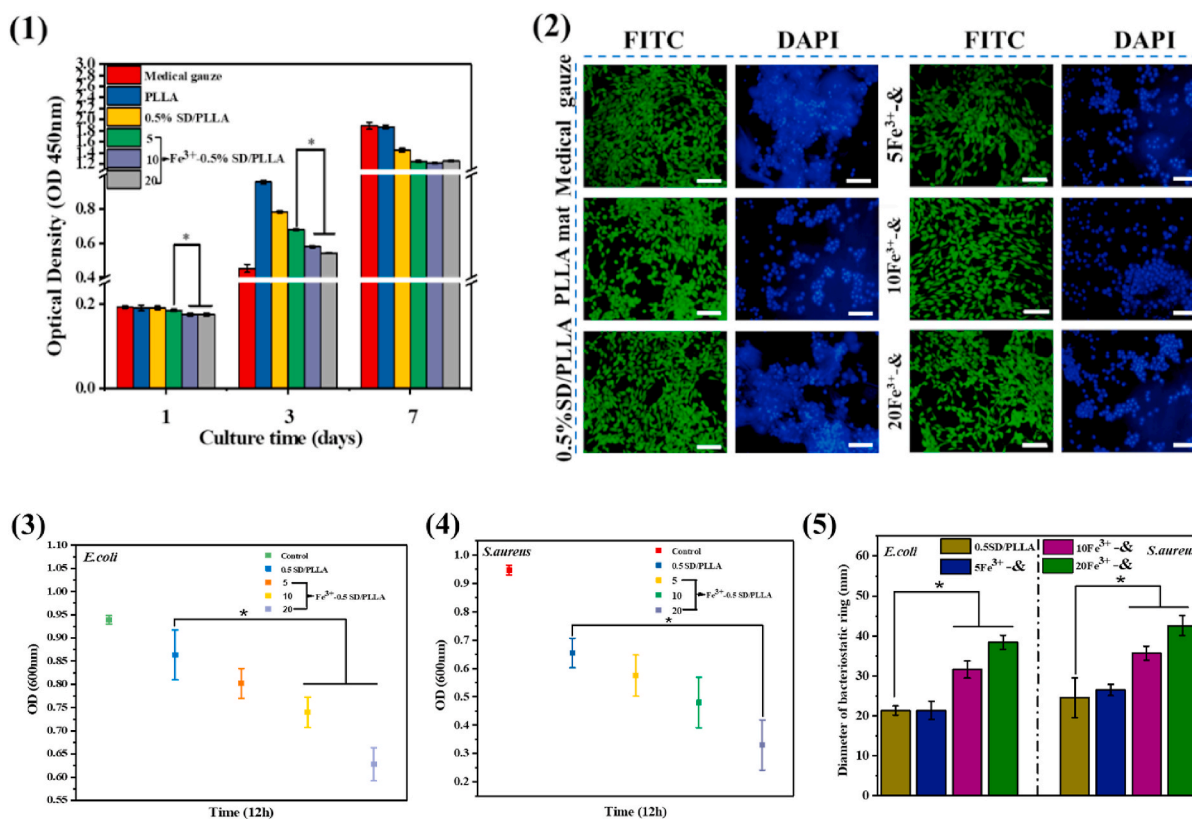

Fig. 6. (1) CCK-8 assay of NIH3T3 osteoblasts cultured on different material substrates (2) Fluorescence micrographs of NIH3T3 cells cultured on different composite material for 3 days and cells were stained with FITC and DAPI, scale bar = 100 μm. (3) Optical density (600 nm) of *E. coli* which co-culture with materials for 12 h (4) Optical density (600 nm) of *S. aureus* which co-culture with materials for 12 h (5) Diameter of bacteriostatic ring formed on solid medium of *E. coli* and *S. aureus*. *present a significantly difference at $P < 0.05$. & representative 0.5SD/PLLA.

materials for both *E. coli* and *S. aureus*. The cause of antibacterial is due to the catechol groups of poly (dopa) on the surface of the PLLA fibre can capture bacterial cells once it is close to the surface and then killed by the quinone groups formed by Fe^{3+} oxidation [73]. Meanwhile, $20Fe^{3+}$-0.5SD/PLLA showed a slightly lower antibacterial ability for *E. coli* than for *S. aureus* because the cytoderm structure of *E. coli* is much more complicated than that of *S. aureus* [74].

3.5. Histocompatibility of composite in vivo

To estimate the histocompatibility of styptic cotton, it was transplanted into the dorsal muscles of mice. Melt spinning PLLA fibre mat, a widely used biocompatible fibre mat, was used as negative control. The results of histological staining with H&E at 1, 7 and 14 days after the material immigrated into muscle are shown in Fig. 7(2). On the 1 day, post-injection, many inflammatory cells were observed, indicating slight inflammation around the material. On day 7, the number of
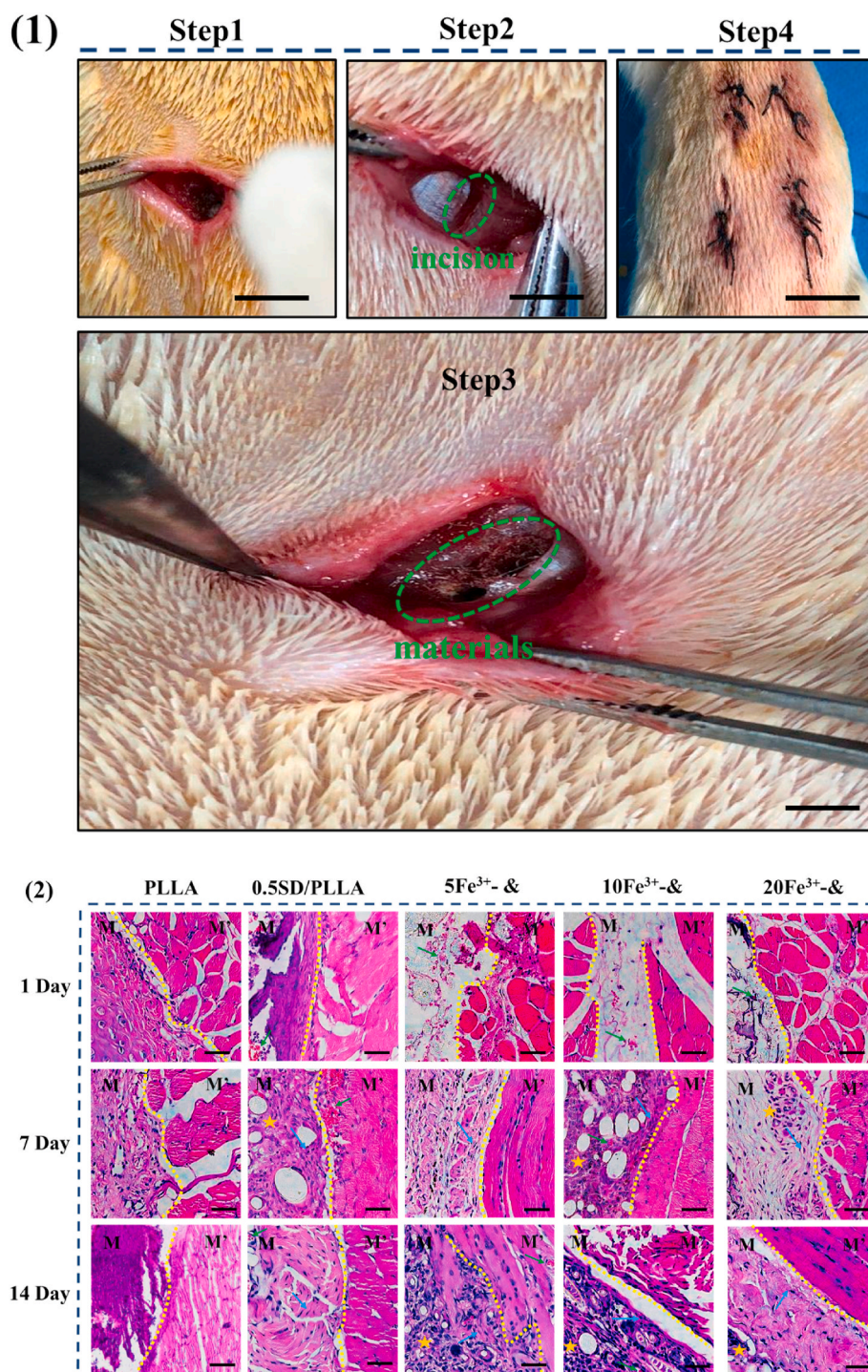
Fig. 7. (1) The procedure of inserting the material into the back muscles of rat, scale bar = 1.5 cm (2) The hematoxylin-eosin staining of muscle tissue for 0, 7, 14 days. M for material, M′ for muscle, neutrophils marked with yellow star, eosinophilic granulocyte marked with green arrows, fibroblasts marked with blue aarows, scale bar = 50 μm & representative 0.5SD/PLLA.

inflammatory cells was significantly reduced and some fibroblasts appeared, suggesting that this material could promote the growth and proliferation of fibroblasts. On day 14, only trace amounts of neutrophils were observed and more fibroblasts appeared. These results indicated that this material could recruit a large number of inflammatory cells and fibroblasts, effectively promote the formation of granulation tissue and play an important role in wound healing.

4. Conclusion

In summary, a novel hemostatic fibrous mat was fabricated. The cotton-like structure, robust hydrophilicity and highly porous structure of SD/PLLA composite led to high water absorption in 0.5SD/PLLA. Furthermore, the nanofibre structure formed by the SD composite on the PLLA fibrous surface promoted platelet adhesion. Hence, benefiting its super water absorption and nanofibre structure on the PLLA fibre surface, 0.5SD/PLLA could quickly cause platelets and blood cells to gather and promote the formation of blood clot to accelerate haemostasis. After Fe^{3+} combined with 0.5SD/PLLA, the hemostatic performance was further improved due to the ability of Fe^{3+} to resist fibrinolysis and trigger the coagulation cascade. In addition, the quinone groups formed by Fe^{3+} oxidation of catechol on pDA presented superior antibacterial properties. When the haemorrhage model of rat liver and rat tail rupture was treated, $20Fe^{3+}$-0.5SD/PLLA showed excellent hemostasis performance. Moreover, $20Fe^{3+}$-0.5SD/PLLA revealed an improvement in cytocompatibility, hemocompatibility and histocompatibility. These results demonstrated that $20Fe^{3+}$-0.5SD/PLLA is a suitable hemostatic product for future clinical and first aid applications.

CRediT authorship contribution statement

Caili Lv: Investigation, Data curation, Writing - original draft. **Linlong Li:** Investigation, Methodology, Software, Visualization, Writing - original draft. **Huanhuan Yan:** Methodology, Software. **Zongliang Wang:** Writing - review & editing. **Zhenxu Wu:** Data curation. **Min Guo:** Validation. **Yu Wang:** Conceptualization, Methodology, Writing - review & editing. **Peibiao Zhang:** Conceptualization, Methodology, Writing - review & editing, Project administration, Funding acquisition, Supervision.

Declaration of competing interest

The authors declare that they have no known competing financial interests or personal relationships that could have appeared to influence the work reported in this paper.

Acknowledgments

Appendix A. Supplementary data

Supplementary data to this article can be found online at https://doi.org/10.1016/j.bioactmat.2021.01.002.

References

[1] A. Shukla, J.C. Fang, S. Puranam, F.R. Jensen, P.T. Hammond, Hemostatic multilayer coatings, Adv. Mater. 24 (4) (2012) 492–+.
[2] L.R. Burnett, J.G. Richter, M.B. Rahmany, R. Soler, J.A. Steen, G. Orlando, T. Abouswareb, M.E. Van Dyke, Novel keratin (KeraStat (TM)) and polyurethane (Nanosan (R)-Sorb) biomaterials are hemostatic in a porcine lethal extremity hemorrhage model, J. Biomater. Appl. 28 (6) (2014) 869–879.
[3] B.J. Eastridge, R.L. Mabry, P. Seguin, J. Cantrell, T. Tops, P. Uribe, O. Mallett, T. Zubko, L. Oetjen-Gerdes, T.E. Rasmussen, F.K. Butler, R.S. Kotwal, J.B. Holcomb, C. Wade, H. Champion, M. Lawnick, L. Moores, L.H. Blackbourne, Death on the battlefield (2001-2011): implications for the future of combat casualty care, J Trauma Acute Care 73 (2012) S431–S437.
[4] D.A. Hickman, C.L. Pawlowski, U.D.S. Sekhon, J. Marks, A. Gupta, Biomaterials and advanced technologies for hemostatic management of bleeding (vol 30, 1700859, 2018), Adv. Mater. 30 (36) (2018).
[5] N. Li, X. Yang, W. Liu, G. Xi, M. Wang, B. Liang, Z. Ma, Y. Feng, H. Chen, C. Shi, Tannic acid cross-linked polysaccharide-based multifunctional hemostatic microparticles for the regulation of rapid wound healing, Macromol. Biosci. 18 (11) (2018), e1800209.
[6] R.N. Udangawa, P.E. Mikael, C. Mancinelli, C. Chapman, C.F. Willard, T. J. Simmons, R.J. Linhardt, Novel cellulose–halloysite hemostatic nanocomposite fibers with a dramatic reduction in human plasma coagulation time, ACS Appl. Mater. Interfaces 11 (17) (2019) 15447–15456.
[7] V.K. Frantz, H.T. Clarke, R. Lattes, Hemostasis with absorbable gauze (oxidized cellulose], Ann. Surg. 120 (1944) 181–198.
[8] Y. Hong, F. Zhou, Y. Hua, X. Zhang, C. Ni, D. Pan, Y. Zhang, D. Jiang, L. Yang, Q. Lin, Y. Zou, D. Yu, D.E. Arnot, X. Zou, L. Zhu, S. Zhang, H. Ouyang, A strongly adhesive hemostatic hydrogel for the repair of arterial and heart bleeds, Nat. Commun. 10 (1) (2019) 2060.
[9] G. Xi, W. Liu, M. Chen, Q. Li, X. Hao, M. Wang, X. Yang, Y. Feng, H. He, C. Shi, W. Li, Polysaccharide-based Lotus seedpod surface-like porous microsphere with precise and controllable micromorphology for ultrarapid hemostasis, ACS Appl. Mater. Interfaces 11 (50) (2019) 46558–46571.
[10] D. Xia, X. Wang, Y. Wang, Y. Wang, H. Meng, L. Li, P. Zhou, S. Xu, Silver-decorated mesostructured cellular silica foams as excellent antibacterial hemostatic agents for rapid and effective treatment of hemorrhage, Mater Sci Eng C Mater Biol Appl 115 (2020) 111105.
[11] J. Luo, Y. Meng, Y. Zheng, K. Xu, C. Li, Fabrication and characterization of Chinese giant salamander skin composite collagen sponge as a high-strength rapid hemostatic material, J. Biomater. Sci. Polym. Ed. 29 (16) (2018) 1933–1948.
[12] L.L. Sun, B.F. Li, W.K. Song, K. Zhang, Y. Fan, H. Hou, Comprehensive assessment of Nile tilapia skin collagen sponges as hemostatic dressings, Mat Sci Eng C-Mater 109 (2020).
[13] Q.Q. Ouyang, T.T. Hou, C.P. Li, Z. Hu, L.M. Liang, S.D. Li, Q.K. Zhong, P.W. Li, Construction of a composite sponge containing tilapia peptides and chitosan with improved hemostatic performance, Int. J. Biol. Macromol. 139 (2019) 719–729.
[14] V. Leszczak, B.S. Smith, K.C. Popat, Hemocompatibility of polymeric nanostructured surfaces, J Biomat Sci-Polym E 24 (13) (2013) 1529–1548.
[15] K.K. Sankaran, K.S. Vasanthan, U.M. Krishnan, S. Sethuraman, Development and evaluation of axially aligned nanofibres for blood vessel tissue engineering, J Tissue Eng Regen Med 8 (8) (2014) 640–651.
[16] A.M. Behrens, B.J. Casey, M.J. Sikorski, K.L. Wu, W. Tutak, A.D. Sandler, P. Kofinas, In situ deposition of PLGA nanofibers via solution blow spinning, ACS Macro Lett. 3 (3) (2014) 249–254.
[17] W. Hu, Z.M. Huang, S.Y. Meng, C.L. He, Fabrication and characterization of chitosan coated braided PLLA wire using aligned electrospun fibers, J. Mater. Sci. Mater. Med. 20 (11) (2009) 2275–2284.
[18] Y. Qiu, Y.Y. Zhu, Y.J. Yan, N. Chen, Z.L. Chen, Study on preparation of fibrinogen-loaded poly (L-lactic) acid nano-fabrics and its haemostatic performance in swine traumatic haemorrhage models, Blood Coagul. Fibrinolysis 25 (5) (2014) 486–491.
[19] H. Lee, S. Ahn, H. Choi, D. Cho, G. Kim, Fabrication, characterization, and in vitro biological activities of melt-electrospun PLA micro/nanofibers for bone tissue regeneration, J. Mater. Chem. B 1 (30) (2013) 3670–3677.
[20] L. Ren, V. Pandit, J. Elkin, T. Denman, J.A. Cooper, S.P. Kotha, Large-scale and highly efficient synthesis of micro- and nano-fibers with controlled fiber morphology by centrifugal jet spinning for tissue regeneration, Nanoscale 5 (6) (2013) 2337–2345.
[21] H. Zhou, Y. Tang, Z. Wang, P. Zhang, Q. Zhu, Cotton-like micro- and nanoscale poly(lactic acid) nonwoven fibers fabricated by centrifugal melt-spinning for tissue engineering, RSC Adv. 8 (10) (2018) 5166–5179.
[22] D.W. Ji, C.F. Xiao, S.L. An, K.K. Chen, Y.F. Gao, F. Zhou, T. Zhang, Completely green and sustainable preparation of PVDF hollow fiber membranes via melt-spinning and stretching method, J. Hazard Mater. 398 (2020).
[23] Q.Q. Wang, W.J. Ma, E.Q. Yin, S.L. Yu, S.C. Wang, H.X. Xiang, D.X. Li, M.F. Zhu, Melt spinning of low-cost activated carbon fiber with a tunable pore structure for high-performance flexible supercapacitors, Acs Appl Energ Mater 3 (9) (2020) 9360–9368.
[24] A.M. Behrens, M.J. Sikorski, T. Li, Z.J. Wu, B.P. Griffith, P. Kofinas, Blood-aggregating hydrogel particles for use as a hemostatic agent, Acta Biomater. 10 (2) (2014) 701–708.
[25] J.J. Rong, M. Liang, F.Q. Xuan, J.Y. Sun, L.J. Zhao, H.Z. Zheng, X.X. Tian, D. Liu, Q. Y. Zhang, C.F. Peng, F. Li, X.Z. Wang, Y.L. Han, W.T. Yu, W. Shuang, Thrombin-loaded alginate-calcium microspheres: a novel hemostatic embolic material for transcatheter arterial embolization, J. Am. Coll. Cardiol. 70 (16) (2017) C190.
[26] J. Cai, X.J. Chen, X.J. Wang, Y.L. Tan, D.D. Ye, Y.T. Jia, P.F. Liu, H. Yu, High-water-absorbing calcium alginate fibrous scaffold fabricated by microfluidic spinning for use in chronic wound dressings, RSC Adv. 8 (69) (2018) 39463–39469.
[27] X. Yang, W. Liu, N. Li, M.S. Wang, N. Liang, I. Ullah, A.L. Neve, Y. Feng, H. Chen, C. C. Shi, Design and development of polysaccharide hemostatic materials and their hemostatic mechanism, Biomater Sci-Uk 5 (12) (2017) 2357–2368.
[28] H.J. Shu, C.X. Wu, K. Yang, T.W. Liu, C. Li, C.L. Cao, Preparation of rapid expansion alginate/silica fiber composite scaffold and application of rapid hemostatic function, Cai Liao Gong Cheng 47 (12) (2019) 124–129.
[29] F.J. Vickers, J.C. Baumgartner, G. Marshall, Hemostatic efficacy and cardiovascular effects of agents used during endodontic surgery, J. Endod. 28 (4) (2002) 322–323.

[30] J. Ebin, The solid carbon dioxide-ferric chloride technic for hemostasis - experimental study of its effectiveness in brain, viscera and superior sagittal sinus, Arch Surg-Chicago 46 (3) (1943) 386–394.

[31] D.Y. Nechipurenko, N. Receveur, A.O. Yakimenko, T.O. Shepelyuk, A. A. Yakusheva, R.R. Kerimov, S.I. Obydennyy, A. Eckly, C. Leon, C. Gachet, E. L. Grishchuk, F.I. Ataullakhanov, P.H. Mangin, M.A. Panteleev, Clot contraction drives the translocation of procoagulant platelets to thrombus surface, Arterioscl Throm Vas 39 (1) (2019) 37–47.

[32] L. Wang, X.H. Zhang, K. Yang, Y.V. Fu, T.S. Xu, S.L. Li, D.W. Zhang, L.N. Wang, C. S. Lee, A novel double-crosslinking-double-network design for injectable hydrogels with enhanced tissue adhesion and antibacterial capability for wound treatment, Adv. Funct. Mater. 30 (1) (2020).

[33] Y.L. Liu, K.L. Ai, L.H. Lu, Polydopamine and its derivative materials: synthesis and promising applications in energy, environmental, and biomedical fields, Chem. Rev. 114 (9) (2014) 5057–5115.

[34] A.L. Gao, F. Liu, L.X. Xue, Preparation and evaluation of heparin-immobilized poly (lactic acid) (PLA) membrane for hemodialysis, J. Membr. Sci. 452 (2014) 390–399.

[35] S. Kim, J.M. Moon, J.S. Choi, W.K. Cho, S.M. Kang, Mussel-inspired approach to constructing robust multilayered alginate films for antibacterial applications, Adv. Funct. Mater. 26 (23) (2016) 4099–4105.

[36] C.-X. Xie, T.-C. Tian, S.-T. Yu, L. Li, pH-sensitive hydrogel based on carboxymethyl chitosan/sodium alginate and its application for drug delivery, J. Appl. Polym. Sci. 136 (1) (2019).

[37] N.Z. Tianlin Gao, Zongliang Wang, Yu Wang, Ya Liu, * yoshihiro ito, Peibiao Zhang*, biodegradable microcarriers of poly(lactideco-glycolide) and nano-hydroxyapatite decorated with IGF-1 via polydopamine coating for enhancing cell proliferation and osteogenic differentiation, Macromol. Biosci. 15 (2015) 1070–1080.

[38] Y. Fang, Y. Xu, Z. Wang, W. Zhou, L. Yan, X. Fan, H. Liu, 3D porous chitin sponge with high absorbency, rapid shape recovery, and excellent antibacterial activities for noncompressible wound, Chem. Eng. J. 388 (2020).

[39] S. Pourshahrestani, E. Zeimaran, N.A. Kadri, N. Gargiulo, S. Samuel, S.V. Naveen, T. Kamarul, M.R. Towler, Gallium-containing mesoporous bioactive glass with potent hemostatic activity and antibacterial efficacy, J. Mater. Chem. B 4 (1) (2016) 71–86.

[40] Z.P. Wang, X. Song, H.P. Ouyang, X.Q. Liu, F.F. Xiang, C. Li, L. Wang, SCANNING TUNNELING MICROSCOPY OBSERVATIONS OF LINK STRUCTURES ON RUTILE TiO2(110)-(1 x 2), Surf. Rev. Lett. 21 (2) (2014).

[41] M.F. Shih, M.D. Shau, M.Y. Chang, S.K. Chiou, J.K. Chang, J.Y. Cherng, Platelet adsorption and hemolytic properties of liquid crystal/composite polymers, Int. J. Pharm. 327 (1–2) (2006) 117–125.

[42] S. Pourshahrestani, E. Zeimaran, N.A. Kadri, N. Gargiulo, H.M. Jindal, S.V. Naveen, S.D. Sekaran, T. Kamarul, M.R. Towler, Potency and cytotoxicity of a novel gallium-containing mesoporous bioactive glass/chitosan composite scaffold as hemostatic agents, ACS Appl. Mater. Interfaces 9 (37) (2017) 31381–31392.

[43] Q. Zhang, C. Qi, H. Wang, X.F. Xiao, Y. Zhuang, S.J. Gu, Y.S. Zhou, L. Wang, H. J. Yang, W.L. Xu, Biocompatible and degradable Bletilla striata polysaccharide hemostasis sponges constructed from natural medicinal herb Bletilla striata, Carbohydr. Polym. 226 (2019).

[44] A.A. Shefa, M. Taz, S.Y. Lee, B.T. Lee, Enhancement of hemostatic property of plant derived oxidized nanocellulose-silk fibroin based scaffolds by thrombin loading, Carbohydr. Polym. 208 (2019) 168–179.

[45] A. El-Salmawy, T. Kitagawa, I.K. Ko, A. Murakami, Y. Kimura, T. Yamaoka, H. Iwata, Preparation and properties of ProNectin F-coated biodegradable hollow fibers, J. Artif. Organs 8 (4) (2005) 245–251.

[46] A. El-Salmawy, Y. Kimura, Properties of a core-sheath conjugate fiber composed of poly(butylene terephthalate) and poly(L-lactic acid), Seni Gakkai Shi 56 (5) (2000) 241–248.

[47] A. El-Salmawy, Y. Kimura, Structure and properties of bicomponent core-sheath fibers from poly(ethylene terephthalate) and biodegradable aliphatic polyesters, Textil. Res. J. 71 (2) (2001) 145–152.

[48] M.A. Bhuiyan, R.V. Pucha, K. Kalaitzidou, 3D RVE Models able to capture and Quantify the Dispersion, agglomeration, and Orientation state of CNT in CNT/PP nanocomposites, Front Mater 3 (2016).

[49] L.E. Flynn, The use of decellularized adipose tissue to provide an inductive microenvironment for the adipogenic differentiation of human adipose-derived stem cells, Biomaterials 31 (17) (2010) 4715–4724.

[50] E.P. Tan, S.Y. Ng, C.T. Lim, Tensile testing of a single ultrafine polymeric fiber, Biomaterials 26 (13) (2005) 1453–1456.

[51] Y. Yan, V. Sencadas, T. Jin, X. Huang, J. Chen, D. Wei, Z. Jiang, Tailoring the wettability and mechanical properties of electrospun poly(l-lactic acid)-poly

[52] C. Ribeiro, V. Sencadas, C.M. Costa, J.L.G. Ribelles, S. Lanceros-Mendez, Tailoring the morphology and crystallinity of poly(L-lactide acid) electrospun membranes, Sci. Technol. Adv. Mater. 12 (1) (2011).

(glycerol sebacate) core-shell membranes for biomedical applications, J. Colloid Interface Sci. 508 (2017) 87–94.

[53] C. Fu, H. Bai, Q. Hu, T. Gao, Y. Bai, Enhanced proliferation and osteogenic differentiation of MC3T3-E1 pre-osteoblasts on graphene oxide-impregnated PLGA–gelatin nanocomposite fibrous membranes, RSC Adv. 7 (15) (2017) 8886–8897.

[54] C.X. Xie, T.C. Tian, S.T. Yu, L. Li, pH-sensitive hydrogel based on carboxymethyl chitosan/sodium alginate and its application for drug delivery, J. Appl. Polym. Sci. 136 (1) (2019).

[55] B. Ates, S. Koytepe, S. Balcioglu, M.G. Karaaslan, U. Kelestemur, S. Gulgen, O. Ozhan, Biomimetic approach to tunable adhesion of polyurethane adhesives through Fe3+ crosslinking and hydrophobic tween units with balance of adhesion/cohesion forces, Int. J. Adhesion Adhes. 95 (2019).

[56] S. Scheja, S. Domanskyi, M. Gamella, K.L. Wormwood, C.C. Darie, A. Poghossian, M.J. Schoning, A. Melman, V. Privman, E. Katz, Glucose-triggered insulin release from Fe(3+) -Cross-linked alginate hydrogel: experimental study and theoretical modeling, ChemPhysChem 18 (12) (2017) 1541–1551.

[57] G. Ascensao, G. Beersaerts, M. Marchi, M. Segata, F. Faleschini, Y. Pontikes, Shrinkage and mitigation strategies to improve the dimensional stability of CaO-FeOx-Al2O3-SiO2 inorganic polymers, Materials 12 (22) (2019).

[58] J. Hua, Z. Li, W. Xia, N. Yang, J. Gong, J. Zhang, C. Qiao, Preparation and properties of EDC/NHS mediated crosslinking poly (gamma-glutamic acid)/epsilon-polylysine hydrogels, Mater Sci Eng C Mater Biol Appl 61 (2016) 879–892.

[59] S.M. Kang, I. You, W.K. Cho, H.K. Shon, T.G. Lee, I.S. Choi, J.M. Karp, H. Lee, One-step modification of superhydrophobic surfaces by a mussel-inspired polymer coating, Angew. Chem. Int. Ed. 49 (49) (2010) 9401–9404.

[60] H. Yin, Z. Tang, Ultrathin two-dimensional layered metal hydroxides: an emerging platform for advanced catalysis, energy conversion and storage, Chem. Soc. Rev. 45 (18) (2016) 4873–4891.

[61] C. Singh, H.K. Sharma, B.C. Sarkar, Influence of process conditions on the mass transfer during osmotic dehydration of coated pineapple samples, J. Food Process. Preserv. 34 (4) (2010) 700–714.

[62] S.W. Yeom, B. You, K. Cho, H.Y. Jung, J. Park, C. Shin, B.K. Ju, J.W. Kim, Silver nanowire/colorless-polyimide composite electrode: application in flexible and transparent resistive switching memory, Sci Rep-Uk 7 (2017).

[63] B. Lipinski, E. Pretorius, H.M. Oberholzer, W.J. van der Spuy, Interaction of fibrin with red blood cells: the role of iron, Ultrastruct. Pathol. 36 (2) (2012) 79–84.

[64] A. Eckly, B. Hechler, M. Freund, M. Zerr, J.P. Cazenave, F. Lanza, P.H. Mangin, C. Gachet, Mechanisms underlying FeCl3-induced arterial thrombosis, J. Thromb. Haemostasis 9 (4) (2011) 779–789.

[65] A.M. Behrens, M.J. Sikorski, T.L. Li, Z.J.J. Wu, B.P. Griffith, P. Kofinas, Blood-aggregating hydrogel particles for use as a hemostatic agent, Acta Biomater. 10 (2) (2014) 701–708.

[66] P.O. Larson, Topical hemostatic agents for dermatologic surgery, J. Dermatol. Surg. Oncol. 14 (6) (1988) 623–632.

[67] P.O. Larson, Topical hemostatic agents for dermatologic surgery - reply, J. Dermatol. Surg. Oncol. 15 (3) (1989) 343.

[68] B.K. Gu, S.J. Park, M.S. Kim, C.M. Kang, J.I. Kim, C.H. Kim, Fabrication of sonicated chitosan nanofiber mat with enlarged porosity for use as hemostatic materials, Carbohydr. Polym. 97 (1) (2013) 65–73.

[69] E.M. Shabanova, A.S. Drozdov, A.F. Fakhardo, I.P. Dudanov, M.S. Kovalchuk, V. V. Vinogradov, Thrombin@Fe3O4 nanoparticles for use as a hemostatic agent in internal bleeding, Sci. Rep. 8 (1) (2018) 233.

[70] V. Milleret, T. Hefti, H. Hall, V. Vogel, D. Eberli, Influence of the fiber diameter and surface roughness of electrospun vascular grafts on blood activation, Acta Biomater. 8 (12) (2012) 4349–4356.

[71] P. Nakielski, F. Pierini, Blood interactions with nano- and microfibers: recent advances, challenges and applications in nano- and microfibrous hemostatic agents, Acta Biomater. 84 (2019) 63–76.

[72] J.C. Marshall, Special issue: sepsis Why have clinical trials in sepsis failed? Trends Mol. Med. 20 (4) (2014) 195–203.

[73] L. Wang, X. Zhang, K. Yang, Y.V. Fu, T. Xu, S. Li, D. Zhang, L.N. Wang, C.S. Lee, A novel double-crosslinking-double-network design for injectable hydrogels with enhanced tissue adhesion and antibacterial capability for wound treatment, Adv. Funct. Mater. 30 (1) (2019).

[74] M.S.M. Eldin, E.A. Soliman, A.I. Hashem, T.M. Tamer, Antimicrobial activity of novel aminated chitosan derivatives for biomedical applications, Adv. Polym. Technol. 31 (4) (2012) 414–428.